NEW BOUNDARY ELEMENT FORMULATION FOR THE SOLUTION OF LAPLACE'S EQUATION

JACQUES LOBRY
Department of General Physics, Faculty of Engineering, University of Mons, Belgium

ABSTRACT
The boundary element method (BEM) is typically used for solving potential problems and has several advantages over the traditional finite element method (FEM). However, the normal derivative of the potential appears explicitly as an unknown, with some inherent ambiguity at the corner nodes. Moreover, the BEM requires time consuming numerical integration (Gaussian quadrature) along the boundary of the domain. In this paper, we propose a new approach of BEM by introducing the weak nodal "cap" flux approach defined in the context of the finite element method. The domain integrals are eliminated at the discrete level by introducing the FEM approximation of the fundamental solutions at every node of the related mesh as basic functions in the Galerkin formulation of the BVP under study. The implementation of this new technique appears to be simpler as no numerical integration on the boundary of the domain is required so that the method leads to a substantially reduced computational burden. Our method is compared to the classical BEM for the numerical solution of the two-dimensional Laplace equation. It is observed that the normal flux presents a better behaviour at corners. A loss of accuracy may occur but it is compensated by a smaller execution time, allowing a finer mesh.
Keywords: finite element method, boundary element method, green functions, electrostatics.

1 INTRODUCTION
The numerical solution of potential boundary value problems (BVP) is traditionally obtained from the finite element method (FEM) or the boundary element method (BEM) that are well documented in the literature as e.g. [1] and [2]. BEM has several advantages over the FEM such as a discretization of the surface rather than the volume, consequently reducing the number of unknown values and the ability of taking into account domains extending to infinity. This method has proved to give very accurate results in particular in case of stress concentration or with re-entrant corner configurations. Conversely to the FEM, the normal derivative of the potential appears explicitly as an unknown value. It is discretized in the same way, e.g. linearly, as the potential along the boundary but appears ill-defined at the corner nodes of the boundary mesh. In order to avoid this problem, the nodes of the two linear elements meeting at the corner can be shifted inside the two elements. Yet it appears as a trick to solve the ambiguity of the flux definition.

In this paper, we propose a new BEM formulation based on the FEM solution of fundamental solutions (Green's functions) [3], [4] and on a rational definition of nodal flux, as presented in the paper of Bossavit [5]. The domain integrals are eliminated by combining the Galerkin formulation of the BVP under study and the one associated to the fundamental solution for Dirac delta loading every node of the related mesh. This is in contrast with the standard BEM that exploit Green's second identity. In order to avoid a huge time consuming FEM computation of nodal Green's functions, which would lead to an inapplicability of the method for open boundary problem anyway, their exact value is used instead as they are known analytically. The main difference with the classical BEM is that finite domain elements connected to the boundary are needed in order to well define the nodal fluxes. This approach leads to a linear system of equations with a fully populated matrix similarly to BEM. The complexity of the method remains as $\mathcal{O}(n^2)$ for the assembly of the system but the implementation is simpler as no numerical integration (Gaussian quadrature) on the

boundary of the domain is required. Our method is compared to both FEM and BEM for the numerical solution of the two-dimensional Laplace equation.

2 MATHEMATICAL FORMULATION

2.1 The classical BEM

The boundary element method has been used for many years for the solution of 2-D and 3-D engineering problems with some advantages over the finite element method such as a reduced mesh task or a natural open problem treatment capability. In BEM, only the boundary of the domain is discretized and the degrees of freedom are typically potential and flux nodal values that are interpolated over the boundary elements. A system of linear equations is derived for the unknown functions at the boundary points and the potential values at internal points in the domain are post-processed. Let us recall the classical boundary formulation for the Laplace equation defined on a 2-D domain Ω ($\partial\Omega = \Gamma_u \cup \Gamma_n$) as illustrated in Fig. 1(a).

$$\nabla^2 u = 0 \text{ in } \Omega, \text{ with } u = u_0 \text{ on } \Gamma_u \quad \text{and} \quad \frac{\partial u}{\partial n} = 0 \text{ on } \Gamma_n. \tag{1}$$
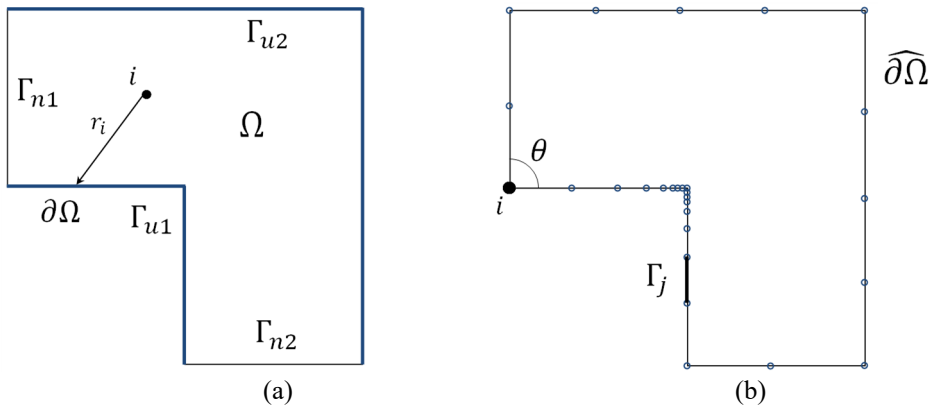
Figure 1:   (a) Typical 2-D domain Ω for the Laplace problem; and (b) Associated boundary element discretization.

In order to establish the formulation, the fundamental solution $\mathcal{G}_i$ regarding the governing equation is employed. It is defined from the Dirichlet problem:

$$\nabla^2 \mathcal{G}_i = -\delta_i \text{ in } \Omega, \quad \text{with } \mathcal{G}_i = \frac{1}{2\pi} \ln \frac{1}{r_i} \text{ on } \partial\Omega, \tag{2}$$

where δ_i is the Dirac delta function at any point i, assumed internal to begin with. Then the domain integrals are eliminated using Green's second identity so that there is obtained:

$$u_i = \oint_{\partial\Omega} \left(u \frac{\partial \mathcal{G}_i}{\partial n} - \mathcal{G}_i \frac{\partial u}{\partial n} \right) d\Gamma. \tag{3}$$

The discretization $\widehat{\partial\Omega}$ of the boundary $\partial\Omega$ into elements Γ_j (Fig. 1(b)) leads to:

$$\hat{u}_i = \sum_{j \in \widehat{\partial\Omega}} \int_{\Gamma_j} \frac{\partial \mathcal{G}_i}{\partial n} \hat{u} \, d\Gamma - \sum_{j \in \widehat{\partial\Omega}} \int_{\Gamma_j} \mathcal{G}_i \hat{q} \, d\Gamma, \tag{4}$$

where $\hat{q}$ denotes the approximate normal derivative. In order to assembly a consistent system of equations, eqn (4) must be written by choosing every node i of the boundary $\widehat{\partial\Omega}$ as the Dirac point. In this situation, a geometric factor c_i is affected to the left-hand side of (4) so that:

$$c_i \, \hat{u}_i = \sum_{j\in\widehat{\partial\Omega}} \int_{\Gamma_j} \frac{\partial G_i}{\partial n} \hat{u} \, d\Gamma - \sum_{j\in\widehat{\partial\Omega}} \int_{\Gamma_j} G_i \, \hat{q} \, d\Gamma. \tag{5}$$

It is equal to the relative part of the Dirac density embedded in the domain Ω at each node i, i.e. the ratio $\theta/2\pi$ (θ is the internal angle at node i – see Fig. 1(b)). This factor is e.g. equal to ½ in case of a smooth boundary and 1 at internal nodes. The boundary potential $\hat{u}$ and flux $\hat{q}$ are typically interpolated linearly on every element Γ_j. The various integrals are either solved analytically or numerically using a standard Gaussian quadrature, depending on whether the node i belongs or not to the element Γ_j. After prescribing the boundary conditions, the procedure leads to a fully populated linear system of equations of which the solution consists of the unknown nodal values $\hat{u}_i$ and $\hat{q}_i$.

The computational effort to construct the matrix is an important part in BEM by contrast with FEM where it is relatively inexpensive to assemble. It scales as $\mathcal{O}(n^2)$ where n is the size of the boundary mesh.

2.2 A new BEM formulation

The finite element analysis of the Laplace problem (1) is based on the Galerkin problem:

$$\int_{\widehat{\Omega}} \nabla\hat{u} \, \nabla N_j = 0 \quad \forall \, j \in \widehat{\Omega} \setminus \widehat{\Gamma}_u, \quad \hat{u} = u_0 \text{ on } \Gamma_u, \tag{6}$$

where the N_j's are the classical nodal basis "hat" functions defined on a mesh $\widehat{\Omega}$ of the domain Ω (Fig. 2). The solution u is approached by:

$$\hat{u} = \sum_{k\in\widehat{\Omega}} N_k \, \hat{u}_k . \tag{7}$$
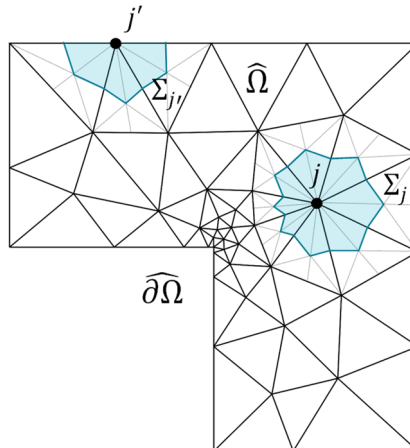
Figure 2: Typical finite element triangular mesh and barycentric boxes Σ_j ("cap" $\Sigma_{j'}$) for an internal (boundary) node j (j').

It leads to a sparse system of linear equations that involves the computation of the integrals of the form:

$$s_{jk} = \int_{\widehat{\Omega}} \nabla N_j \, \nabla N_k \, d\Omega. \tag{8}$$

On the other hand, in the paper of Bossavit [5], the term:

$$\int_{\widehat{\Omega}} \nabla \hat{u} \, \nabla N_j \, d\Omega = \sum_{k\in\widehat{\Omega}} s_{jk} \, \hat{u}_k = \Phi_{\hat{u},\Sigma_j} \quad \forall j \in \widehat{\Omega} \tag{9}$$

is shown to be equal to the inward flux of $\nabla \hat{u}$ across the "box" Σ_j associated to node j in the dual mesh obtained from the barycentric subdivision of the primal mesh as shown in Fig. 2. Those weak "box" fluxes vanish for nodes $j \in \partial\Omega \setminus \Gamma_u$ due to eqn (6) and are interpreted as a part of the flux of $\nabla \hat{u}$ through "caps" associated to Dirichlet boundary nodes like $j' \in \Gamma_u$. This gives rise to the best ("variationally" correct) estimate of surface charges in electrostatics for e.g. the direct computation of capacitance. In this case, the result is shown to be exactly the same as the approximate energy value $\hat{\mathbf{u}}^t\mathbf{S}\,\hat{\mathbf{u}}$, where $\mathbf{S} = (s_{jk})$ is the stiffness matrix of the problem. In the following, the parameters Φ_{Σ_j} are used in place of the approximation of the normal derivative $\hat{q}$ given by the standard BEM.

In order to eliminate the domain integral, the 2-D fundamental solution $\mathcal{G}_i$ of Laplace's equation is employed, as in the standard BEM. In spite of the singularity of the solution, i.e. $\mathcal{G}_i$ lies outside Sobolev space H^1, a FEM solution exists [3], [4] and is derived from the Galerkin problem associated to eqn (2):

$$\int_{\widehat{\Omega}} \nabla\hat{\mathcal{G}}_i \, \nabla N_j \, d\Omega = \int_{\widehat{\Omega}} \delta_i \, N_j \, d\Omega \quad \forall j \in \widehat{\Omega} \setminus \widehat{\partial\Omega}, \quad \hat{\mathcal{G}}_i = \frac{1}{2\pi}\ln\frac{1}{r_i} \text{ on } \widehat{\partial\Omega}. \tag{10}$$

Consider point i be any internal node of the mesh $\widehat{\Omega}$ then, in the same way as for $\hat{u}$ we can write the nodal approximation:

$$\int_{\widehat{\Omega}} \nabla\hat{\mathcal{G}}_i \, \nabla N_j \, d\Omega = \Phi_{\hat{\mathcal{G}}_i,\Sigma_j} \quad \forall j \in \widehat{\Omega}, \tag{11}$$

that is the equivalent of (9). Note that we have $\Phi_{\hat{\mathcal{G}}_i,\Sigma_i} = 1$. The FEM solution $\hat{\mathcal{G}}_i$ can be expressed as:

$$\hat{\mathcal{G}}_i = \sum_{j\in\widehat{\Omega}} N_j \, \hat{\mathcal{G}}_{i,j} = \sum_{j\in\widehat{\Omega}\setminus\widehat{\Gamma}_u} N_j \, \hat{\mathcal{G}}_{i,j} + \sum_{j\in\widehat{\Gamma}_u} N_j \, \hat{\mathcal{G}}_{i,j}. \tag{12}$$

It is permitted to write, using successive eqns (7), (12), (8), (6) and (9):

$$\int_{\widehat{\Omega}} \nabla\hat{u} \, \nabla\hat{\mathcal{G}}_i \, d\Omega = \sum_{j\in\widehat{\Omega}\setminus\widehat{\Gamma}_u}\Big(\sum_{k\in\widehat{\Omega}} s_{jk} \, \hat{u}_k\Big) \hat{\mathcal{G}}_{i,j} + \sum_{j\in\widehat{\Gamma}_u}\Big(\sum_{k\in\widehat{\Omega}} s_{jk} \, \hat{u}_k\Big) \hat{\mathcal{G}}_{i,j} = \sum_{j\in\widehat{\Gamma}_u}\Phi_{\hat{u},\Sigma_j} \, \hat{\mathcal{G}}_{i,j}. \tag{13}$$

Conversely, using eqns (7), adapted to $\hat{\mathcal{G}}_i$, (11) instead of (9) and the boundary conditions for u, we can write:

$$\int_{\Omega} \nabla\hat{\mathcal{G}}_i \, \nabla\hat{u} \, d\Omega = \sum_{j\notin\partial\Omega}\Big(\sum_{k\in\widehat{\Omega}} s_{jk} \, \hat{\mathcal{G}}_{i,k}\Big) \hat{u}_j + \sum_{j\in\partial\Omega}\Big(\sum_{k\in\widehat{\Omega}} s_{jk} \, \hat{\mathcal{G}}_{i,k}\Big) \hat{u}_j$$
$$= \hat{u}_i + \sum_{j\in\widehat{\Gamma}_n}\Phi_{\hat{\mathcal{G}}_i,\Sigma_j} \, \hat{u}_j + \sum_{j\in\widehat{\Gamma}_u}\Phi_{\hat{\mathcal{G}}_i,\Sigma_j} \, \hat{u}_0. \tag{14}$$

Equating (13) and (14), we obtain the following expression where the domain integral is eliminated as expected:

$$\hat{u}_i + \sum_{j\in\widehat{\Gamma}_n}\Phi_{\hat{\mathcal{G}}_i,\Sigma_j} \, \hat{u}_j + \sum_{j\in\widehat{\Gamma}_u}\Phi_{\hat{\mathcal{G}}_i,\Sigma_j} \, \hat{u}_0 = \sum_{j\in\widehat{\Gamma}_u} \hat{\mathcal{G}}_{i,j} \, \Phi_{\hat{u},\Sigma_j}. \tag{15}$$

A consistent linear system of equations is derived by writing eqn (15) for all the nodes i belonging to the boundary $\widehat{\partial\Omega}$. In this situation, the boundary condition of the problem (2) must be changed as:

$$\mathcal{G}_i = \frac{1}{2\pi} \ln \frac{1}{r_i} \text{ on } \partial\Omega \backslash \{i\} \quad \text{and} \quad \frac{\partial \mathcal{G}_i}{\partial n} = 0 \text{ at } \{i\}, \tag{16}$$

so that the Galerkin formulation becomes:

$$\int_\Omega \nabla \hat{\mathcal{G}}_i \, \nabla N_j \, d\Omega = \delta_{ij} \, c_i \quad \forall j \in (\widehat{\Omega} \backslash \widehat{\partial\Omega}) \cup \{i\}, \quad \hat{\mathcal{G}}_i = \frac{1}{2\pi} \ln \frac{1}{r_i} \text{ on } \widehat{\partial\Omega} \backslash \{i\}, \tag{17}$$

where δ_{ij} is the common Kronecker symbol and c_i is the same geometric factor as used in classical BEM. In the FEM context it can be easily shown that:

$$c_i = \Phi_{\hat{\mathcal{G}}_i, \Sigma_i} \quad \text{and} \quad c_i + \sum_{j \in \partial\widehat{\Omega} \backslash \{i\}} \Phi_{\hat{\mathcal{G}}_i, \Sigma_j} = 0, \tag{18}$$

i.e. the Gauss law at the discrete level.

Finally the boundary element scheme amounts to solve simultaneously:

$$c_i \, \hat{u}_i + \sum_{\substack{j \in \widehat{\Gamma}_n \\ \neq i}} \Phi_{\hat{\mathcal{G}}_i, \Sigma_j} \, \hat{u}_j + \sum_{\substack{j \in \widehat{\Gamma}_u \\ \neq i}} \Phi_{\hat{\mathcal{G}}_i, \Sigma_j} \, \hat{u}_0 = \sum_{j \in \widehat{\Gamma}_u} \hat{\mathcal{G}}_{i,j} \, \Phi_{\hat{u}, \Sigma_j} \qquad \forall \, i \in \widehat{\partial\Omega}, \tag{19}$$

or, in matrix form:

$$\mathbf{H}.\hat{\mathbf{u}} = \mathbf{G}.\boldsymbol{\Phi}_{\hat{u}}. \tag{20}$$

Rearranging terms, it yields a linear system that is to be solved for unknown potential values $\hat{u}_j$ on $\widehat{\Gamma}_n$ and flux values $\Phi_{\hat{u},\Sigma_j}$ on $\widehat{\Gamma}_u$.

At this point, the exact FEM solution of the BVP (1) is obtained since we have derived the eqns (19) by choosing test functions as a linear combination of the hat functions N_j in (13) and (14). It is clear that there is no interest in doing so. Moreover, this requires the computation of the FEM approximations $\hat{\mathcal{G}}_i$ that is highly time consuming. The trick is then to use the exact fundamental solutions $\mathcal{G}_i$ instead of $\hat{\mathcal{G}}_i$, i.e. we use the interpolant:

$$\mathcal{G}_{i,I} = \sum_{j \in \widehat{\Omega}} N_j \, \mathcal{G}_i(j) = \sum_{j \in \widehat{\Omega}} N_j \frac{1}{2\pi} \ln \frac{1}{r_{ij}}, \tag{21}$$

where r_{ij} is the distance between nodes i and j. Due to the singularity, the infinite value $\mathcal{G}_i(i)$ is replaced by a value $\mathcal{G}_{i,i}^*$ from the pair of eqns (18), i.e.:

$$\hat{c}_i = \sum_{k \neq i} s_{ik} \, \mathcal{G}_i(k) + s_{ii} \, \mathcal{G}_{i,i}^* \tag{22a}$$

and

$$\hat{c}_i + \sum_{j \in \partial\widehat{\Omega} \backslash \{i\}} \left(\sum_{k \neq i} s_{jk} \, \mathcal{G}_i(k) + s_{ji} \, \mathcal{G}_{i,i}^* \right) = 0. \tag{22b}$$

Indeed, (22a) express the "cap" flux at any boundary node i and (22b) stands for the weak flux inside the domain Ω along the boundary $\widehat{\partial\Omega}$, due to the Dirac delta δ_i. Solving simultaneously these equations leads to the desired value $\mathcal{G}_{i,i}^*$, along with an approximate factor $\hat{c}_i$. The modified geometric factor $\hat{c}_i$ is not equal to the exact one obtained previously. Although we could force $\hat{c}_i \triangleq c_i$, the numerical simulations indicate a better accuracy by using the above statements. This is probably due to the consistency brought by the discrete Gauss laws given by (22a) and (22b).

It is important to notice that it is not necessary to mesh the whole domain since the internal nodes disappear in the boundary formulation (19). A single layer of finite elements along the boundary is sufficient. This is even mandatory in the case of an open boundary problem. In this case, the right-hand side of eqn (22b) is equal to unity due to the integral at infinity.

Finally, notice that the computational effort to construct the matrix scales as $\mathcal{O}(n^2)$ as in classical BEM. However it does not require any integration so that a reduction by a factor of about N_G is expected when using a N_G-point Gaussian quadrature.

3 NUMERICAL RESULTS

The method has been applied to several simple electrostatic problems in order to estimate the basic performance of our numerical scheme. We have implemented both our method and the classical BEM with MATLAB® software for the ease of analysis and exploitation of the results. The boundary integrals are calculated with a Gaussian quadrature method with seven points in our BEM implementation. COMSOL Multiphysics® has been used for the generation of the various meshes required by the simulations.

3.1 A closed geometry example: the square coaxial capacitor

First of all, we consider the square coaxial air capacitor arrangement depicted in Fig. 3. The governing equation is given by eqn (1), up to the absolute permittivity ε_0. The prescribed potential values on the Dirichlet boundaries Γ_{u1} and Γ_{u2} are $u_1 = 1$ V and $u_2 = 0$ V, respectively. The problem can be analysed either on the whole geometry or on a reduced geometry considering some symmetry. In the following, both approaches are investigated in order to assess the various corner effects on the normal flux value such as the re-entrant corner and the Dirichlet to Neumann change in boundary condition.
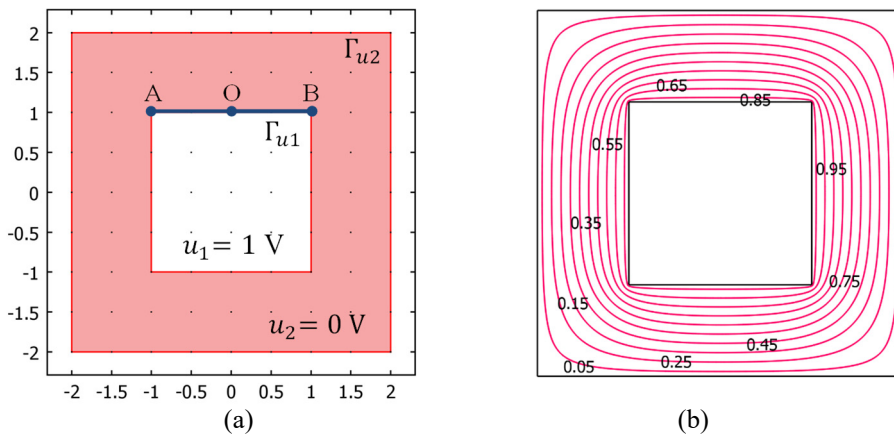
Figure 3: A square coaxial configuration. (a) Geometry; and (b) Solution.

3.1.1 Full geometry configuration

We consider the complete geometry of the problem of which a finite element mesh is shown in Fig. 4(a). Uniform meshing is applied in order to get a reference convergence behaviour. A comparison has been carried out between our method and the classical BEM. First, we have computed the distribution of the surface charge density $\sigma = \varepsilon_0.\partial u/\partial n$ along the inner

Dirichlet boundary. Classical BEM gives directly this result since it relates to the $\hat{q}_i$ parameters at every node of the boundary mesh. In our method, the nodal normal derivatives can be reasonably deduced from the nodal "cap" flux value $\Phi_{\hat{u},\Sigma_i}$ by using the following ansatz:

$$\hat{q}_i = \frac{\Phi_{\hat{u},\Sigma_i}}{s_i}, \tag{23}$$

where the cross section s_i is chosen as shown in Fig. 4(b), though it is not strictly correct as explained in [5].
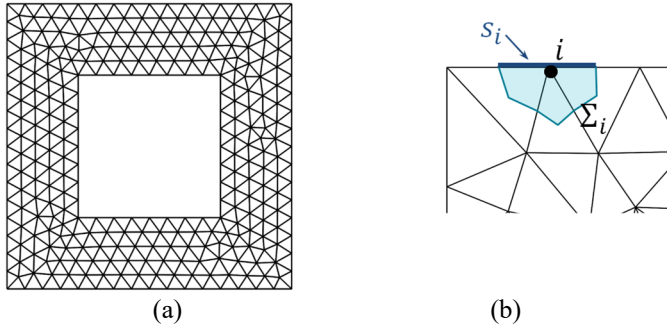
Figure 4: (a) FE-mesh; and (b) Computation of the normal derivative from nodal "cap" flux.

The results are plotted in Fig. 5 along the path AB depicted in Fig. 3(a) for a boundary mesh of size $n = 768$, superimposed to the "exact" one, obtained from a FEM simulation with a very fine mesh. It is clear that the normal derivative at re-entrant corners A and B presents a bad accuracy with standard BEM though it is better with the new technique. The computation of the surface charge value Q distributed on the Dirichlet boundary Γ_{u1} has also been performed. It is obtained by summing the "cap" flux values along the boundary in the proposed method, and a boundary integration of the normal flux $\hat{q}$ for BEM. The reference value $Q = 10.23409$ C is obtained analytically following the method described in [6]. Fig. 6(a) presents the convergence results where it can be observed a loss in accuracy despite the better behaviour of the normal derivative reported in Fig. 5. However, as explained in Section 2, since the computational effort is reduced in a factor of N_G chosen equal to 7 here, our technique remains competitive in this respect as shown in Fig. 6(b) where the results of BEM have been shifted to the right accordingly that is, taking into account the complexity of $\mathcal{O}(n^2)$, by $\log(\sqrt{N_G})$.

The charge has also been computed by the finite element method. It can be derived from either the electrostatic energy W, i.e. $Q = 2W/U$, or by summing the "cap" flux values along the boundary. Both method leads exactly to the same value for the charge Q as suggested in [5]. The convergence of FEM appears to be very close to our method as observed in Fig. 6(a).

3.1.2 L-shaped geometry configuration

A quarter of the geometry of the coaxial configuration is now considered as presented in Fig. 7(a). From symmetry argument, the Neumann condition is applied on the parts Γ_{n1} and Γ_{n2}. Again, a uniform triangle mesh is applied. The distribution of the normal derivative on the path OB (Fig. 7(b)) is again computed. Here we point out a discrepancy at point O due to
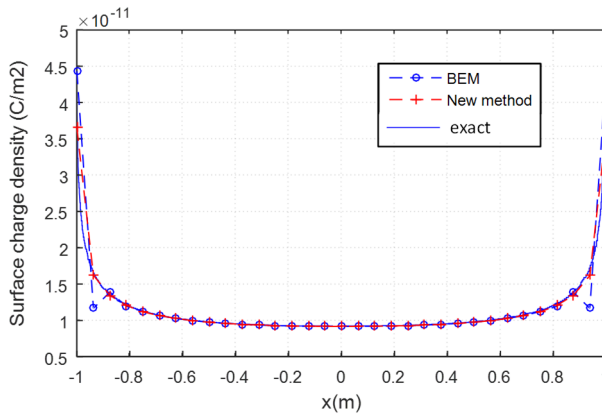
Figure 5:   Square coaxial configuration: surface charge density distribution along path AB ($n = 768$). Comparison of numerical (symbols) and exact (full line) results.

(a)   (b)
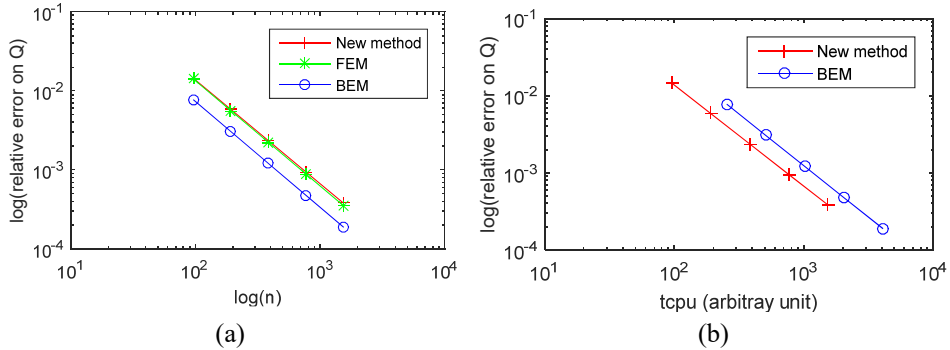
Figure 6:   Square coaxial configuration: relative error on the surface charge Q with respect to (a) The size n; and (b) The computational burden t_{cpu}.

the change in boundary condition as well as at re-entrant corner B as in Section 3.1.1. The computation of the surface charge value Q distributed on the Dirichlet boundary Γ_{u1} gives the error results shown in Fig. 8. Now it is clear that our method outperforms the classical methods for the computation of this global quantity. The loss in accuracy of standard BEM is due to the underestimation of the normal flux at corner O. The results obtained from a FEM analysis are also plotted and lie between the two BEM techniques.

The same comparison study has been conducted for the potential value at internal points 1, 2 and 3 that are chosen as indicated in Fig. 7(a). The numerical results are compared to reference values that are deduced from a FEM analysis with a dense triangulation: $u_1 = 0.8787$ V, $u_2 = 0.2865$ V, $u_3 = 0.7916$ V. We now restrict the comparison to the new method and the BEM. Fig. 9 shows the results for equal computational burden. They are not better for all points with our method. Clearly, accuracy at point 3 is far better due to a bad accuracy at the nearby Dirichlet/Neumann corner with BEM but is not so good for point 1 although re-entrant corner presents problem with BEM. From an execution time point of view, the comparison indicates that our method remains competitive.
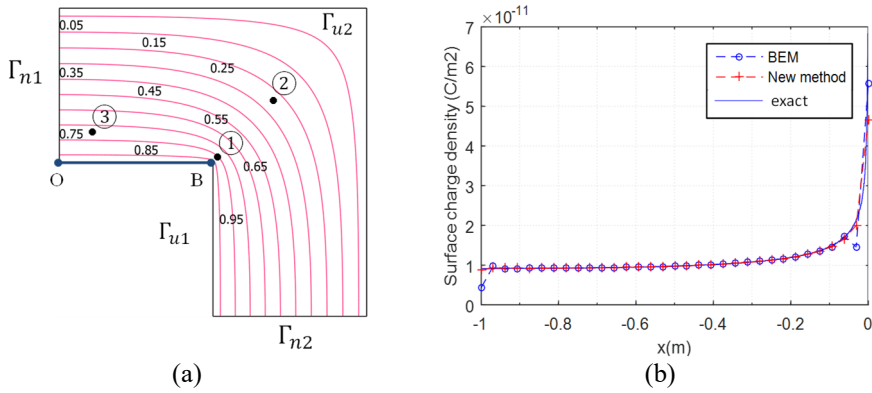
Figure 7:   L-shaped configuration. (a) Solution; and (b) Surface charge density distribution along path OB ($n = 248$). Comparison of numerical (symbols) and exact (full line) results.
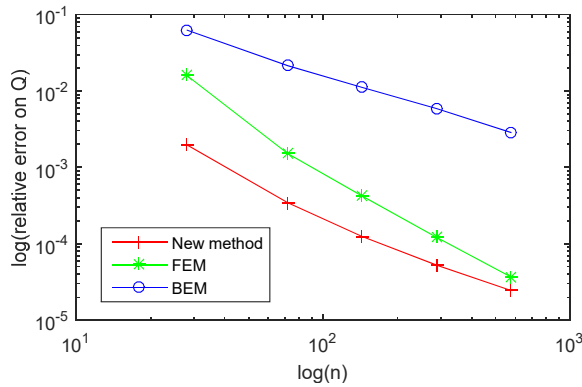
Figure 8: L-shaped configuration: relative error on the surface charge.
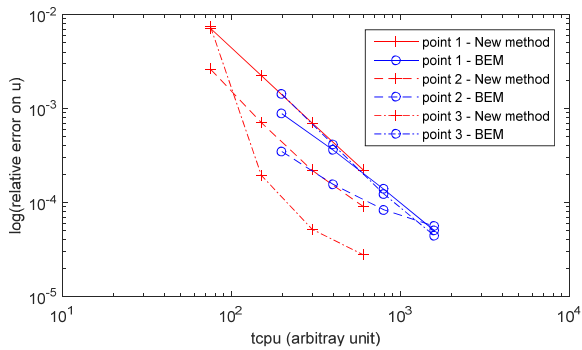
Figure 9:   L-shaped configuration: relative error on the potential value at internal points 1, 2 and 3.

3.2 An open boundary problem

As an advantage of BEM lies in the ability of treating open boundary problems, we consider the situation of a symmetric parallel wire capacitor as shown in Fig. 10. The prescribed potential values on the Dirichlet boundaries Γ_{u1} and Γ_{u2} are $u_1 = -1/2$ V and $u_2 = 1/2$ V, respectively. Similar numerical analysis has been conducted concerning the surface charge density along the boundary Γ_{u1} and the related global charge Q. Classical electromagnetism gives analytical results for these quantities so that an error analysis can be performed. The results are shown in Fig. 11.
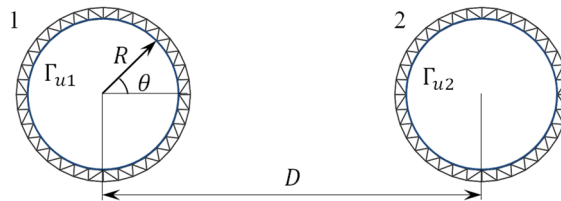
Figure 10: Parallel wire capacitor ($R = 0.2$ m, $D = 1$ m).
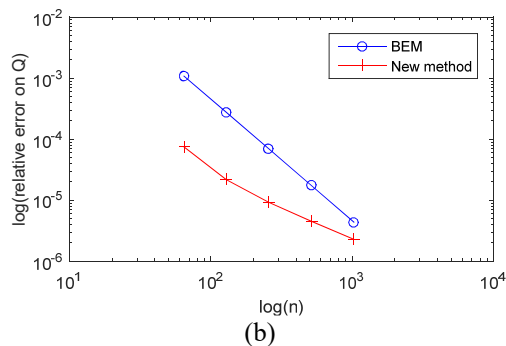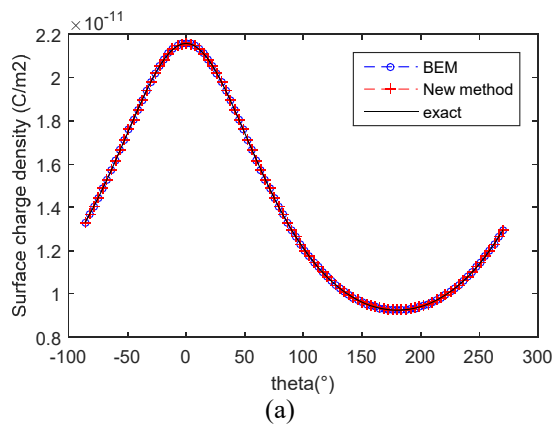
Figure 11: Parallel wire capacitor. (a) Surface charge density ($n = 192$); and (b) Error on the charge Q on conductor 1.

   Fig. 11(a) shows that surface charge density is very well reproduced by both methods. From Fig. 11(b), comparison of errors on the total charge value is shown to be lower with our method pointing out a better accuracy though convergence rate appears to be higher with standard BEM for more refined mesh. This last point should be further investigated.

4 DISCUSSION AND CONCLUSION

In this paper, we have proposed a new BEM formulation based on the FEM solution of the fundamental solution and on a "variationally" correct definition of nodal flux. The main difference with the classical BEM is that at least a layer of finite domain elements connected to the boundary is needed. The implementation is simpler as no numerical integration on the boundary of the domain is required. Numerical examples have been conducted in order to compare both our method and the classical BEM. The new scheme exhibits the advantage of an unambiguous definition of the normal flux when corners are present in the geometry. However, the computation of global quantities such as the charge or potential at internal nodes are sometimes less accurate. Further investigation is needed in order to analyse the influence of the quality of the finite element mesh that is necessary along the boundary. Indeed, numerical experiments show that it affects the accuracy. This point requires some improvements and clarifications. Yet the method is competitive since the computational burden is significantly reduced. Extension of the method to the Poisson equation and multi-domain configurations are straightforward and have been tested but not presented in the paper. Moreover, the proposed technique can be easily interfaced with finite elements in a FEM/BEM coupling since the "cap" flux is intrinsically related to the FEM. This will be the subject of a future paper.

REFERENCES

[1] Silvester, P.P. & Ferrari, R.L., *Finite Elements for Electrical Engineers*, Cambridge University Press, 1996.
[2] Brebbia, C.A. & Dominguez, J., *Boundary Elements: An Introductory Course*, WIT Press: Southampton and Boston, 1992.
[3] Hartmann, F., *Green's Functions and Finite Elements*, Springer, 2013.
[4] Araya, R., Behrens, E. & Rodriguez, R., A posteriori error estimates for elliptic problems with Dirac delta source terms. *Numerische Mathematik*, **105**(2), pp. 193–216, 2006.
[5] Bossavit, A., How weak is the "weak solution" in finite element methods? *IEEE Transactions on Magnetics*, **34**(5), pp. 2429–2432, 1998.
[6] Riblet, J.H., Expansion for the capacitance of a square in a square with a comparison. *IEEE Transactions on Microwave Theory and Techniques*, **44**(2), pp. 338–340, 1996.